Validation of the DSCOVR Spacecraft Mission Space Weather Solar Wind Products

Paul T. M. Loto'aniu[1,2], K. Romich[1,2], W. Rowland[1,2], S. Codrescu[1,2], D. Biesecker[3], J. Johnson[1,4], H.J. Singer[4], A. Szabo[5], M. Stevens[6]

[1]Cooperative Institute for Research in Environmental Sciences, University of Colorado Boulder, Boulder, CO, USA
[2]National Centers for Environmental Information, National Oceanic and Atmospheric Administration, Boulder, CO, USA
[3]National Environmental Satellite, Data, and Information Service, National Oceanic and Atmospheric Administration, Boulder, CO, USA
[4]Space Weather Prediction Center, National Oceanic and Atmospheric Administration, Boulder, CO, USA
[5]Goddard Space Flight Center, National Aeronautics and Space Administration, Greenbelt, MD, USA
[6]Center for Astrophysics, Harvard and Smithsonian, Cambridge, MA, USA

Key Points:

- We validate the DSCOVR operational space weather data products
- Magnetic field data showed good statistical agreement with *Wind* and ACE data
- Solar wind velocity GSE v_x-component and density also showed good statistical agreement with *Wind* and ACE data

Corresponding author: Paul T.M. Loto'aniu, `paul.lotoaniu@noaa.gov`

Abstract

In this paper, we present a statistical validation of the DSCOVR solar wind data in the operational space weather archive. The DSCOVR observations of the interplanetary magnetic field (IMF), solar wind velocity, density, and temperature were hourly averaged and compared to measurements from NASA's ACE and *Wind* spacecraft. Hourly averages, in general, show good correlations between the satellites for the IMF, solar wind velocity GSE v_x-component, and density. During the period covered by this study (spanning from late July 2016, when DSCOVR went operational, to the end of 2020), the DSCOVR products show no clear evidence of permanent degradation. However, for plasma parameters there were periods of disagreement with ACE and *Wind*. The correlation coefficients (Pearson's r) calculated over the entire study period were similar or the same between DSCOVR versus *Wind* and DSCOVR versus ACE. For comparisons between DSCOVR and *Wind*, the IMF B_x and B_y GSE r were 0.94 and 0.96, respectively, while r for the IMF GSE B_z-component was 0.88. For solar wind velocity, r was found to be 0.96 for the GSE v_x-component, compared with 0.30 for v_y and 0.33 for v_z. For density, r was found to be 0.84. DSCOVR density observations tend to overestimate compared to *Wind* values when the solar wind densities are low (below ∼5 /cc), while agreement between the two spacecraft on IMF measurements tend to increase with decreasing spatial separation.

Plain Language Summary

We present a statistical validation of space weather operational products derived from measurements onboard a National Oceanic and Atmospheric Administration (NOAA) spacecraft orbiting at about 1.5 million kilometers towards the Sun from Earth. Spacecraft observations of the solar wind magnetic field, velocity, density, and temperature were hourly averaged and compared to measurements from two other spacecraft in similar orbits. Hourly averages, in general, show good correlations between the spacecraft for solar wind magnetic field, the main component of velocity and density. However, for solar wind plasma parameters there were periods of disagreement with the other two spacecraft. The NOAA spacecraft density observations tend to overestimate when compared to one of the other spacecraft measurements when the solar wind densities are low, while agreement between these two spacecraft on magnetic field measurements tend to increase with decreasing spacecraft separation.

Keywords

DSCOVR, Space Weather, Solar Wind

1 Introduction

The NOAA Deep Space Climate Observatory (DSCOVR) mission was launched in February 2015 to the 1st Lagrange point (L1), which is located about 1.5 million kilometers from Earth, towards the sun, along the Sun-Earth line. The DSCOVR mission is a NOAA space weather operational mission that provides and sustains the United States' real-time solar wind monitoring capabilities, which are critical to the accuracy and lead time of NOAA's space weather alerts and forecasts. NOAA funded NASA to refurbish the DSCOVR spacecraft and solar wind instruments, develop the command and control portion of the ground segment, and manage the launch and activation of the satellite. The United States Air Force funded and managed the SpaceX Falcon 9 launch services for DSCOVR. On 7 June 2015, DSCOVR reached its final L1 destination, and in late October 2015, after checkout and post-launch testing, NOAA officially took command of the DSCOVR satellite. DSCOVR became the NOAA operational L1 solar wind mon-

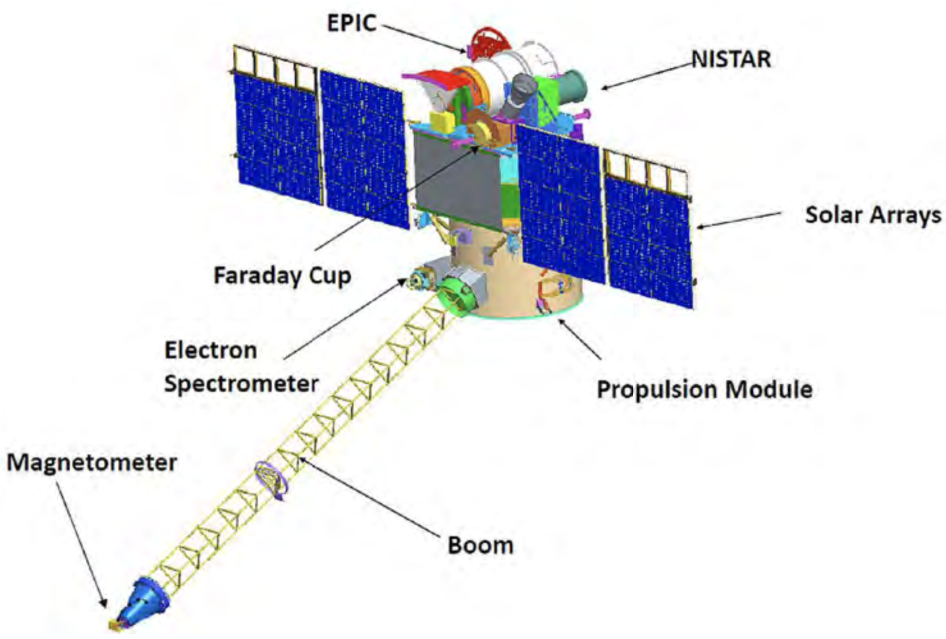

Figure 1. Diagram of the DSCOVR spacecraft with instruments indicated (Szabo, 2014).

itor on 27 July 2016 at 16:00 UTC when it began providing data for space weather forecasting at the NOAA Space Weather Prediction Center (SWPC).

The main science payloads onboard DSCOVR are the PlasMag suite, which includes the solar wind monitoring plasma (Faraday Cup) and magnetometer instruments, the Earth-observing NIST Advanced Radiometer (NISTAR), and the Earth Polychromatic Imaging Camera (EPIC). Figure 1 shows the spacecraft with instrument payloads indicated. Of interest in this study is the PlasMag suite, which measures the solar wind particles and the interplanetary magnetic field (B_{IMF}) for NOAA space weather predictions. There is also an electrostatic analyzer (ESA) spectrometer on DSCOVR, which is not a requirement by NOAA for space weather operations.

NOAA operates DSCOVR from its NOAA Satellite Operations Facility (NSOF) in Suitland, Maryland and distributes the data to its users and partner agencies. NOAA processes the space weather data, providing products and forecasts through the NOAA-SWPC in Boulder, Colorado, and archives the data at the NOAA National Centers for Environmental Information (NCEI), also in Boulder, Colorado. NASA is responsible for processing the EPIC data.

The focus of this study is the validation of the NOAA-NCEI DSCOVR space weather or PlasMag instrument suite archive. The validation effort is restricted to the 1-minute or lower resolution data products and covers the years 2016-2020. We validate against data from NASA's Advanced Composition Explorer (ACE) and *Wind* spacecraft missions, which were both located at L1 during the validation interval.

When interpreting the results presented, it should be kept in mind that the NOAA-NCEI DSCOVR archive contains data collected during real-time NOAA operations, whereas the ACE and *Wind* datasets may have undergone further post-processing to improve science quality. Hence, we expect to observe more issues such as missing data in the DSCOVR archive. This is further emphasized by the fact that the DSCOVR spacecraft has expe-

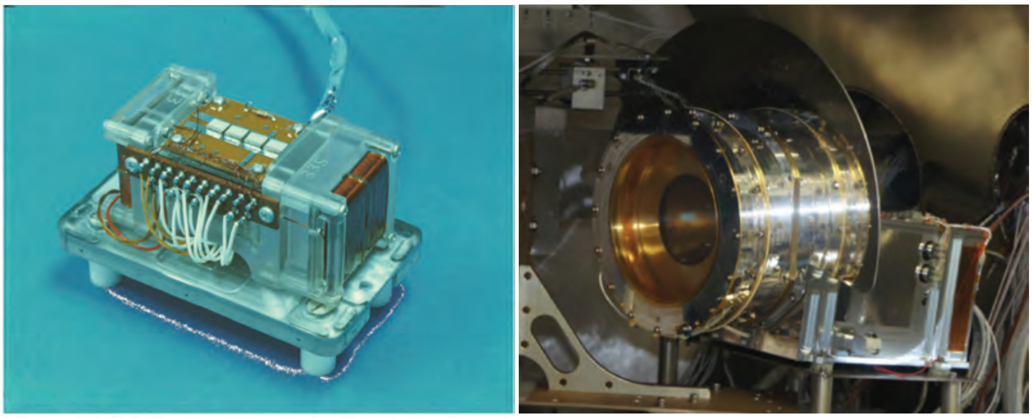

Figure 2. Left: A photo of the DSCOVR magnetometer instrument (Szabo, 2015). Right: a photo of the DSCOVR Faraday Cup instrument (Kasper et al., 2013).

Table 1. The MAG Observational Requirements

Parameter	Requirements	Performance
B_{IMF}	3-axis vector observation in-situ	N/A
Accuracy	1.0 nT/axis	0.2 nT/axis
Sample Rate	1 vectors/min/axis	50 vectors/sec/axis
Range	$\pm 0.1 - 100$ nT	$0.004 - 65500$ nT

rienced multiple issues since commissioning that affect both the quality and availability of the space weather data.

In the following paper, Section 2 describes the DSCOVR PlasMag instruments. Section 3 discusses the methodology for the validation and data availability, while Section 4 shows the results. Finally, conclusions are discussed in Section 5.

2 The DSCOVR Space Weather Instruments

2.1 The Magnetometer

The DSCOVR tri-axial fluxgate magnetometer (MAG), which measures the interplanetary vector magnetic field (B_{IMF}) and is shown on the left in Figure 2, is located at the tip of a 4.0 m boom to minimize the effect of spacecraft fields. The MAG was provided by the NASA Goddard Space Flight Center (GSFC) in Greenbelt, Maryland and underwent pre-launch instrument- and spacecraft-level tests also at NASA-GSFC (Connerney, 2013). These tests establish instrument pre-launch calibration parameters such as zero offsets, gains or scale factors, alignment, noise, and spacecraft magnetic signature at the sensor location.

Table 1 shows the requirements and performance of the MAG (Szabo & Koval, 2016). Currently, the NOAA-SWPC operational requirement is for the B_{IMF} product at 1-minute cadence. However, the MAG instrument on DSCOVR samples at 50 samples/sec. The instrument has multiple ranges, with the highest reaching 65500 nT for ground calibration.

Table 2. Observational requirements of the DSCOVR Faraday Cup.

Parameter	Requirements	Initial Performance
Velocity Range	200 – 1250 km/s	168 – 1340 km/s
Velocity Accuracy	20%	2%
Density Range	1 – 100 cm^{-3}	0.22 – 219 cm^{-3}
Density Accuracy	20%	1%
Temperature Range	4x10^4-2x10^6 K	3.9x10^4-7.3x10^6 K
Temperature Accuracy	20%	<9%
Cadence	60 s	0.25 s

On-orbit, the DSCOVR spacecraft underwent a series of rolls in order to estimate MAG zero offsets. Independently, offsets were also determined using solar wind Alfvenic wave rotation methods (Davis & Smith, 1968; Belcher et al., 1969; Belcher, 1973) to ensure consistent offset values (Szabo, 2015). In operations, the spacecraft continues to undergo maneuvers about every six weeks to redetermine offsets, and the Alfvenic method is also used to verify results and determine the roll axis offset. The calibration analysis is performed by NASA-GSFC and updated offsets are sent to SWPC for operational use.

The space weather products created from the MAG observations are the total magnetic field, the vector magnetic field in GSE and GSM coordinates, and the magnetic field θ and ϕ angles. The NOAA archive MAG products are daily files at full resolution (50 Hz), 1-second cadence, and 1-minute cadence. However, since the operational product is the 1-minute data, here we use the archived 1-minute vector magnetic field data.

2.2 The Faraday Cup

The DSCOVR Faraday Cup (FC) is a retarding potential particle detector that provides high time resolution solar wind proton bulk properties (wind speed, density, and temperature) (Szabo, 2015). The FC measures the flux of positively charged solar wind particles as a function of their kinetic energy per charge. The instrument, which is shown on the right in Figure 2, consists primarily of a circular collector plate, divided into three independent 120° sectors, positioned behind a high-voltage grid (Stevens et al., 2014). Apart from the segmentation of the collector, the DSCOVR Faraday Cup is very similar to the *Wind* Faraday Cup described by Ogilvie et al. (1995).

The FC's observational requirements and performance are shown in Table 2. Performance exceeds requirements for all parameters. However, on-orbit analysis showed that the FC data underperforms during certain low solar wind conditions. This is described in § 4.2.

3 Data and Methodology

3.1 Data Description

The solar wind parameters derived from DSCOVR data that are validated in this study against ACE and *Wind* data are those most important to current NOAA space weather operations, namely, the 1-minute resolution IMF magnetic field, speed, proton density, and temperature. These parameters are archived in the DSCOVR Level 2 1-minute averaged magnetometer and Faraday Cup instrument-derived netCDF data files; these files were obtained through the DSCOVR Space Weather Data Portal maintained by NOAA's

National Centers for Environmental Information (NCEI) [`https://www.ngdc.noaa.gov/dscovr/`]. A full list of the NOAA-NCEI archived DSCOVR space weather data products can be found on the portal website. The products have a code that uniquely identifies each product within the filenames; for this study they are `m1m` (1-minute averaged magnetometer data) and `f1m` (1-minute Faraday Cup data). Users can also plot summaries of the DSCOVR data on the portal. It should be noted that real-time, operational, solar wind data can be obtained from NOAA's Space Weather Prediction Center at `https://www.swpc.noaa.gov/`.

The ACE and *Wind* data used in this analysis were obtained from NASA's Coordinated Data Analysis Web (NASA-CDAWeb) [`https://cdaweb.gsfc.nasa.gov/index.html/`]. In order to compare with ACE and *Wind* data over the lifetime of the DSCOVR mission, the DSCOVR data were averaged to hourly and monthly values. The NASA-CDAWeb ACE data products used were the 1-hour magnetic field (`AC_H2_MFI`) and solar wind parameters (`AC_H2_SWE`). For *Wind*, hourly averages were available for the magnetic field only (`WI_H0_MFI`), while the solar wind particle data were derived from the 92-s resolution data products (`WI_K0_SWE`).

There are higher quality products on the NASA-CDAWeb. For example, the *Wind* `WI_H1_SWE` product was produced with human in-the-loop. However, we use the `K0` data because it is more similar in terms of processing steps to the real-time DSCOVR archive.

The time period considered for validation spans from 26 July 2016 (the earliest availability of NCEI DSCOVR Level 2 data) to 31 December 2020. For each satellite, we examine magnetic field strength (B_x, B_y, B_z), solar wind velocity (v_x, v_y, v_z), proton density, and proton temperature. Geocentric Solar Ecliptic (GSE) coordinates are used for both vector quantities. In the case of *Wind*, an additional step is required to find temperature values, since the parameter stored in the data repository is not temperature but most probable thermal speed (i.e., $v_{\mathrm{th}} = \sqrt{2kT/M}$, where k is Boltzmann's constant and M is the mass of a single proton). Hence the Kelvin temperature is given by $T = [M{v_{\mathrm{th}}}^2/(2k)] \times 10^6$, with the 10^6 factor included because v_{th} is provided in km/s.

3.2 Data Availability

With the exception of the ACE Magnetic Field Investigation (MFI) data (which at time of download were unavailable on CDAWeb past 24 November 2020) and the ACE Solar Wind Electron Proton Alpha Monitor (SWEPAM) data (which at time of download were unavailable on CDAWeb past 30 June 2019), the analyses described in this paper were conducted over the full range of dates indicated above. Missing data or fill values are excluded from the study period. Additional manipulations were sometimes necessary, such as regridding to a regular timestamp that matches across datasets.

Figure 3 displays the DSCOVR B_z (GSE) magnetic field component and solar wind v_x (GSE) velocity component from 26 July 2016 to 31 December 2020, with periods of data missing from the DSCOVR MAG and FC data archives indicated by the red regions. These regions represent dates for which <75% of the available data are usable and comprise 17.2% and 17.7% of all dates considered for the MAG and FC archives, respectively.

The bulk of the DSCOVR data issues occur in the second half of 2019 and early 2020. This was due to problems with DSCOVR's Miniature Inertial Measurement Unit (MIMU) that caused mission operations to place the spacecraft in an extended safe hold mode. The MIMU issues were not resolved until early March 2020, when DSCOVR returned to nominal operations. In addition to the MIMU issues, soon after commissioning in June 2015 DSCOVR experienced spurious reboots, which reset the spacecraft and placed it into safe hold mode. The resets occurred infrequently and was fixed in mid-

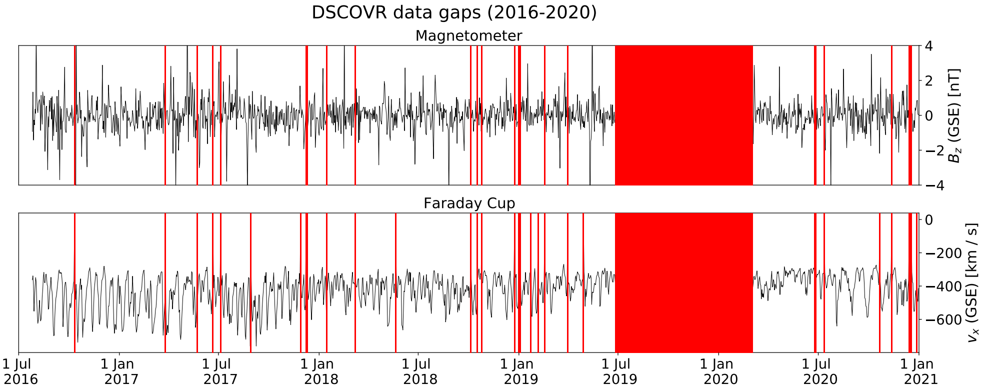

Figure 3. Visualization of DSCOVR MAG B_z component (top) and Faraday Cup solar wind v_x component (bottom) data, showing date ranges for which DSCOVR data were available for this study. The red regions represent dates for which <75% of the available data are usable.

2019. Other technical issues have occurred from time-to-time that have resulted in short periods of data loss.

3.3 Statistical Methodology

We compute hourly resolution times series using DSCOVR, ACE and *Wind* data. (Note, the year 2020 was excluded from the ACE/SWEPAM time series due to the lack of available data from NASA CDAWeb.) Using hourly-averaged data, we perform linear regressions on the eight parameters of interest across each pair of satellites (DSCOVR-ACE, DSCOVR-*Wind*, and *Wind*-ACE). Since there is measurement error in each dataset, we use orthogonal-distance regression (which accounts for error in both dependent and independent variables) rather than simple ordinary-least-squares regression, which assumes a predictor variable that is free from error. Unlike ordinary-least-squares regression, which determines the equation of a linear regression line by minimizing the vertical distance from each data point to the line, orthogonal regression seeks to minimize the orthogonal distance from each data point to the line (Boggs et al., 1988). The regression analysis returns the line of best fit $y = ax + b$. We also compute the Pearson correlation coefficient r to assess the strength of the relationship, i.e., the degree to which changes in one variable correspond to changes in the other.

In addition to determining correlations over the nearly five years of available data, we also estimate r-values for each month of data to visualize the evolution of the correlation strength for a given parameter over a multi-year period. This can provide information on instrument degradation or other instrument issues in one or both satellites. It can also be an indicator of the effects of spacecraft separation on correlation strength. We investigate variations in correlation strength in the context of (1) relative position, (2) solar wind speed, and (3) proton density. Using the hourly averages generated previously, we determine monthly averages for spacecraft separation (i.e., the physical distance between satellites in three-dimensional space) as well as the ambient solar wind parameters as measured by *Wind*. This produces a month-by-month time series of the same length as the series of parameter r-values, which can then be compared, using a second Pearson's r calculation, as an initial assessment of the degree to which fluctuations in correlation strength between spacecraft measurements correspond to fluctuations in the parameter of interest.

We also investigate whether DSCOVR over- or under-estimates parameter values as compared to *Wind*, and under what physical conditions this tends to occur. For each of the solar wind plasma parameters, as well as the z-component of the IMF, we compute ratios of hourly averages as measured by DSCOVR and *Wind* (i.e., one DSCOVR/*Wind* data point for each hour from 26 July 2016 00:00 to 31 December 2020 23:00). These are sorted into bins based on solar wind speed (i.e., $|v| = \sqrt{v_x^2 + v_y^2 + v_z^2}$) and proton density, both as measured by *Wind*, and means and standard deviations are determined for each bin.

4 Validation Results

4.1 Comprehensive Regressions

Figure 4 shows scatterplots of hourly averaged magnetic field component data across different pairs of satellites over the full date range for which DSCOVR data were available (2016-2020). Orthogonal-distance regression was used to estimate shown r values and lines of best fit. The r values are consistently high (above 0.8) in all cases, indicating that in general the DSCOVR magnetometer measurements, at least hourly averaged, are in good agreement with ACE and *Wind* observations. In addition, the slope of the line-of-best fit is $\sim$1.0 for all comparisons, showing that there is no significant offset between DSCOVR, ACE and *Wind* magnetic field observations.

Corresponding scatterplots and regressions for solar wind velocity components are shown in Figure 5. Agreement among the three satellites is very strong (≥ 0.96) for the v_x-component. As with the magnetic field components, the slope of each v_x trendline is nearly 1.0 and the y-intercepts are nearly zero. However, there are periods of poor agreement in the v_x-component comparisons as shown between -400 and -200 km/s in the top panels; these will be examined in § 4.2. The r-values for the v_y and v_z component comparisons are lower across all satellite pairs, although for *Wind*-ACE the r-value is higher than either for DSCOVR-ACE or DSCOVR-*Wind*. The slopes of the v_y and v_z trendlines all deviate significantly from unity, but show some consistency between v_y and v_z.

In Figure 6, we display regression results for proton density and temperature. *Wind* versus ACE exhibit the strongest correlations ($r = 0.95$ for density and 0.93 for temperature). The trendline slopes for all three density comparisons are close to unity; this is also the case for the *Wind*-ACE temperature comparison, but the slopes for the temperature comparisons involving DSCOVR are both above 3.

4.2 Monthwise Correlations

Figure 7 displays time series of DSCOVR-*Wind* r-values for B_z, v_x, proton density, and temperature, calculated for each month between July 2016 and December 2020. Despite some fluctuation from month to month, the monthwise correlations are typically strong for B_z, v_x, and density (following generally accepted convention, we define a strong correlation as $|r| > 0.7$, a moderate correlation as $0.5 < |r| < 0.7$, and a weak correlation as $|r| < 0.5$.) The vertical lines mark the occurrence of several software and ground processing patches designed to improve the performance of the Faraday Cup (J. Johnson, private communication).

For B_z, the correlation strength reaches its minimum ($r = 0.65$) in January 2019, which is the only month in which it falls below 0.7. For v_x, the only month in which r falls below 0.7 is August 2017, although additional local minima appear in April 2018 ($r = 0.78$) and December 2020 ($r = 0.79$). For density, 89% of all monthwise r-values are above 0.7, with the lowest ($r = 0.56$) appearing in November 2020. The fluctuations in correlation strength are more pronounced for temperature, with r-values ranging from

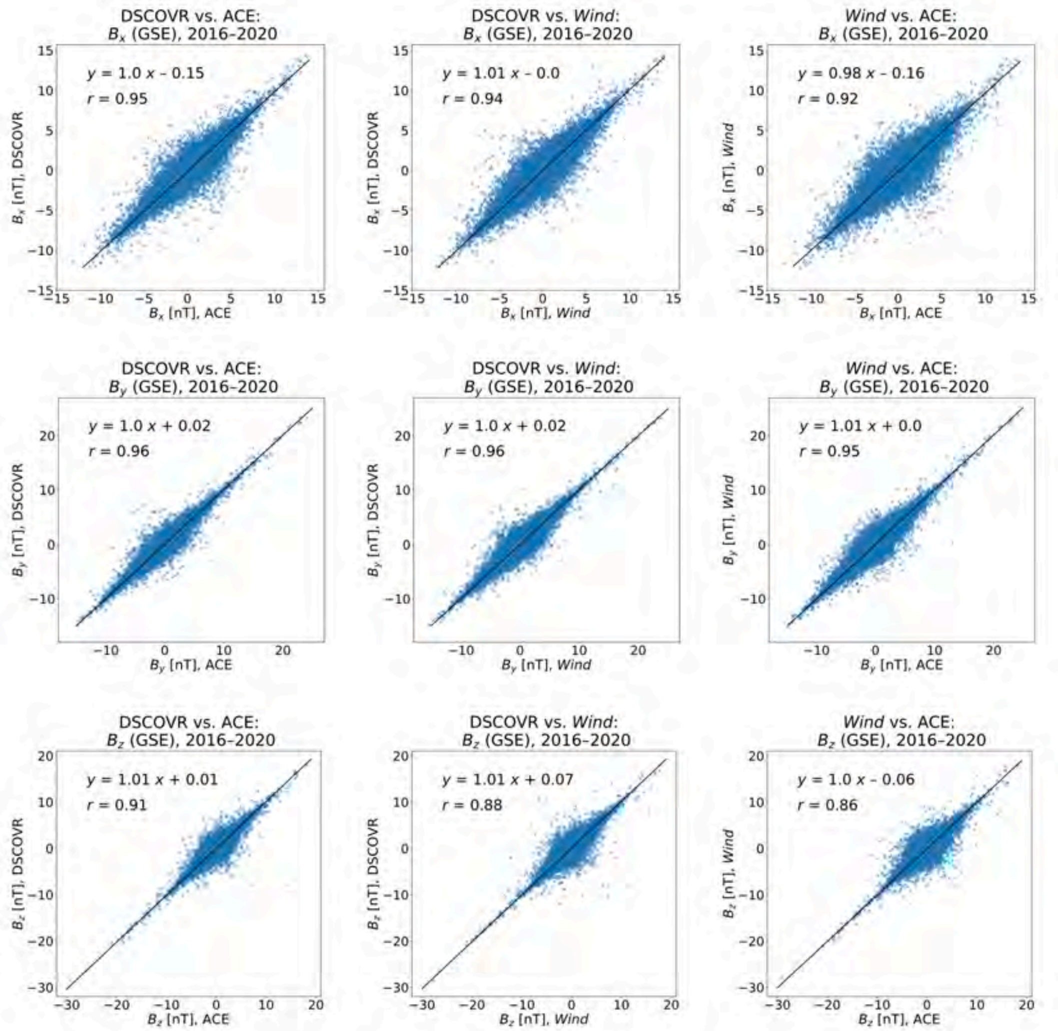

Figure 4. Scatterplots and best-fit lines for hourly average B_x (top), B_y (middle), and B_z (bottom) values across each satellite pair. The DSCOVR-ACE scatterplots contain 31,416 data points from 2016 to 2020; the DSCOVR-*Wind* scatterplots contain 32,129 data points from 2016 to 2020; and the *Wind*-ACE scatterplots contain 37,747 data points from 2016 to 2020. Trendline equations and correlation coefficients (Pearson's r) are indicated on each panel.

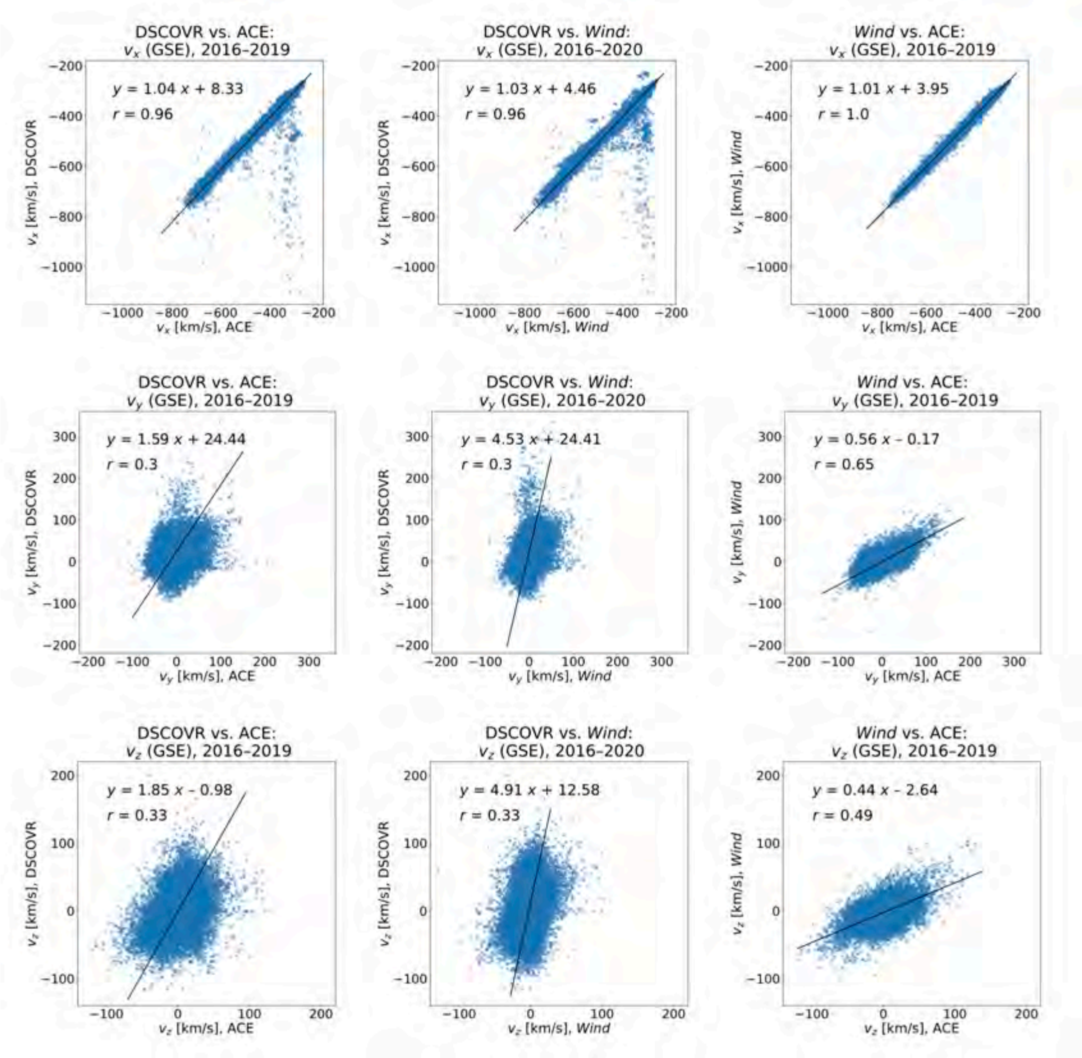

Figure 5. Scatterplots and best-fit lines for hourly average v_x (top), v_y (middle), and v_z (bottom) values across each satellite pair. The DSCOVR-ACE scatterplots contain 24,529 data points from 2016 to 2019; the DSCOVR-*Wind* scatterplots contain 31,430 data points from 2016 to 2020; and the *Wind*-ACE scatterplots contain 25,189 data points from 2016 to 2019. Trendline equations and correlation coefficients (Pearson's r) are indicated on each panel.

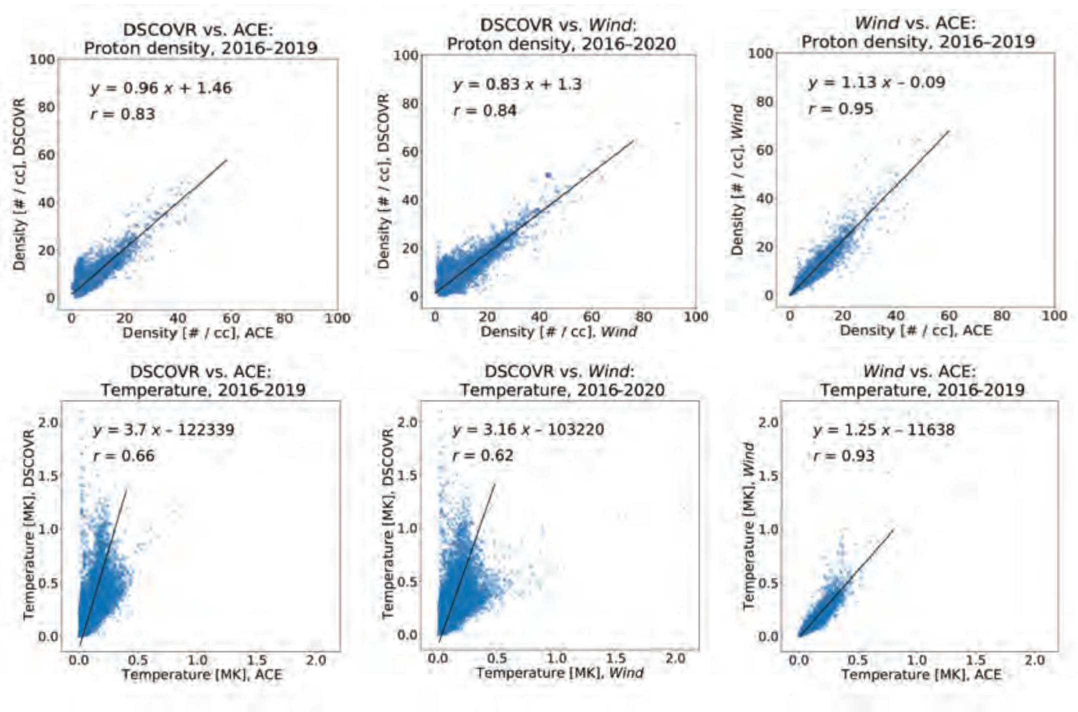

Figure 6. Upper panels: Scatterplots and best-fit lines for hourly average proton density values across each satellite pair. Lower panels: Same as (a) but for hourly average temperature values. Lines of best fit and correlation coefficients (Pearson's r) are also shown. For upper panels - the DSCOVR-ACE, DSCOVR-*Wind* and *Wind*-ACE plots contain 13571, 31430, and 13867 data points, respectively. For lower panels - The DSCOVR-ACE, DSCOVR-*Wind* and *Wind*-ACE plots contain 24080, 31430 and 24,738 data points, respectively. A small number of extreme outliers are excluded from the plots shown.

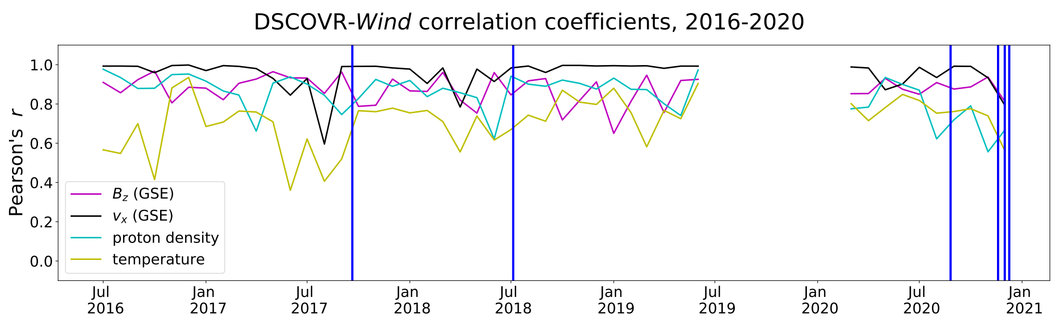

Figure 7. Time series of DSCOVR-*Wind* r values for B_z, v_x, proton density, and temperature, overlaid with blue lines indicating dates of Faraday Cup patches. Between July 2019 and February 2020, usable DSCOVR data were unavailable, leading to the gap visible here. A total of 46 data points for each parameter are represented in this plot.

0.36 to 0.94. Although correlations for all variables shown in the figure tend to decrease at the end of the period studied, as noted above, there were other periods where correlation values dipped.

Biesecker and Johnson (2018) gave a summary of the status of the DSCOVR data and stated that the FC data did not meet requirements during periods of low solar wind density. The 2017 and 2018 patches were expected to have some success in correcting this problem. However, faulty grounding in the FC required changes to its operating mode, and those changes have caused gradual degradation over the years in the quality of the FC data at low solar wind speeds. This is confounded by less accurate background subtractions when the solar wind signal is low. Since these issues mainly occur during low solar wind speed periods, this probably explains the lack of conclusive evidence in figure 7 of overall science data degradation over the mission. Analyzing data through 2021 and beyond would help determine if the decreased correlations observed at the end of the study period are indicative of more long-term degradation.

Quantifying the casual relationship between periods of decreased correlation in figure 7 and all FC issues is beyond the scope of this study. However, the major cause of occasional dips in v_x correlation, observed on August 2017, April 2018, and December 2020, is well understood. For each month, significant discrepancies between DSCOVR and *Wind* v_x spanned only a few days (August 26–29, 2017; April 15–25, 2018; and December 1–8, 2020), with good agreement throughout the rest of the month. Figure 8 shows DSCOVR and *Wind* v_x values, overlaid with concurrent density measurements, for a few days in August 2017 and December 2020. When the solar wind is slow, warm or sparse the FC can fail to resolve the peak amplitude of the solar wind signal, which leads to larger errors in v_x determination (M. Stevens, private communication). Difficulties calculating accurate background subtractions during low solar wind conditions further compound the errors. The top panels of Figure 5 also shows this effect with large spreads in DSCOVR v_x during low ACE and *Wind* $|v_x|$ values.

We did attempt to establish a correlation between low densities and dips in v_x correlation for each of the three time periods. From December 1–8, 2020, the difference between the v_x measurements tends to be higher during periods of low density; we find a moderate-to-strong negative correlation ($r = -0.68$) between ambient density and v_x difference (i.e., $|v_{x,\mathrm{DSCOVR}} - v_{x,Wind}|$). This effect is not clearly observed for the other two periods of poor agreement; for August 26–29, 2017 and April 15–25, 2018, we find $r = -0.20$ and $r = -0.09$, respectively.

In Table 3, we present the results of an additional correlation analysis, which probes for covariance between monthwise DSCOVR-*Wind* r-values and corresponding monthly averages of spacecraft separation, solar wind speed (as measured by *Wind*), and proton density (as measured by *Wind*). By "speed" here we mean the magnitude of the velocity, i.e., $v = \sqrt{v_x^2 + v_y^2 + v_z^2}$. In most cases, these relationships are very weak ($|r| < 0.3$) or nonexistent ($|r| \approx 0$), although a moderate negative correlation ($r = -0.66$) exists between correlation strength for B_z and spacecraft separation. This indicates that agreement between the DSCOVR and *Wind* B_z measurements tends to decrease when the satellites are farther apart. We also find a moderate positive correlation ($r = 0.51$) between the DSCOVR-*Wind* density correlation strength, which means the DSCOVR-*Wind* density comparisons tend to agree more when *Wind* density increases.

4.3 Differences Based on Ratios

In Figure 9 (top), we display plots of DSCOVR-*Wind* proton density ratios (i.e., $N_{\mathrm{DSCOVR}}/N_{Wind}$) that have been classified into three bins based on solar wind speed (i.e., $v = \sqrt{v_x^2 + v_y^2 + v_z^2}$) as measured by *Wind*. Adopting the thresholds used by King and Papitashvili (2005), we distinguish between slow (< 350 km/s), moderate ($350 -$

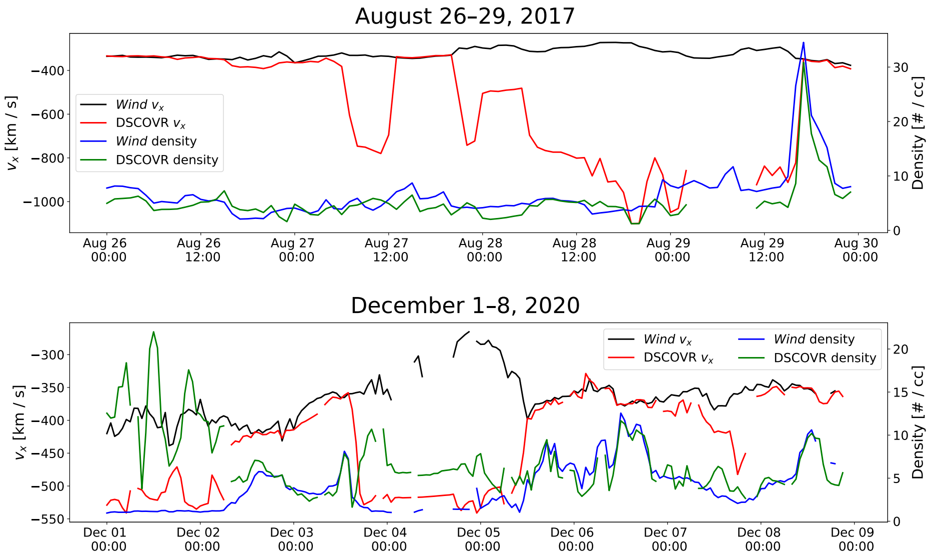

Figure 8. *Top*: DSCOVR (red) and *Wind* (black) v_x values during a period in August 2017 that showed strong disagreement for v_x. *Wind* and DSCOVR density values are shown in blue and green, respectively. There is no significant correlation between *Wind* density and the absolute difference between DSCOVR and *Wind* v_x values during this four-day period. *Bottom*: DSCOVR (red) and *Wind* (black) v_x values during a period of particularly poor alignment in December 2020. *Wind* and DSCOVR density values are shown in blue and green, respectively. There is a moderate negative correlation ($r = -0.68$) between *Wind* density and the absolute difference between DSCOVR and *Wind* v_x values during this eight-day period.

Table 3. Comparison of DSCOVR-*Wind* correlation strength for the four parameters in Figure 7 (one data point for each month from July 2016 to December 2020) against monthly averages of spacecraft separation, solar wind speed (as measured by *Wind*), and proton density (as measured by *Wind*). The values in the table are the correlation coefficients (Pearson's r) for each time series combination.

	r (B_z)	r (v_x)	r (density)	r (temperature)
Average separation	−0.66	−0.09	0.10	0.20
Average speed (*Wind*)	0.14	0.06	0.00	−0.32
Average density (*Wind*)	−0.08	0.09	0.51	0.29

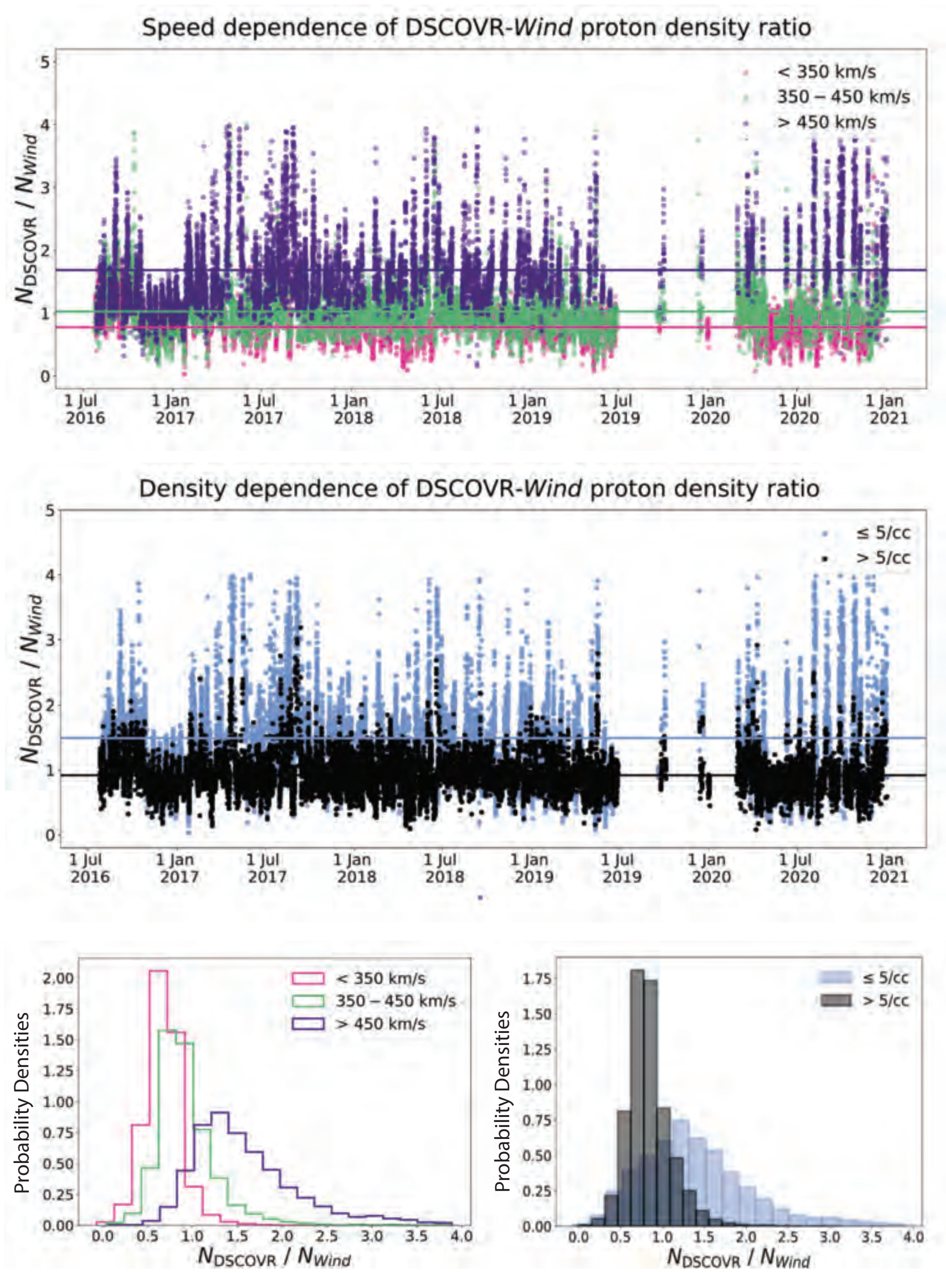

Figure 9. *Top*: Time series of DSCOVR-*Wind* proton density ratios categorized by solar wind speed as measured by *Wind*. Ratios are computed from hourly averages spanning the full range of this analysis (2016−2020). Mean values are indicated by horizontal lines. *Bottom*: Normalized probability density functions (PDFs) for each category ($n_{\text{bins}} = 20$ in each case). The "slow" PDF (<350 km/s) represents 8,998 data points; the "moderate" PDF (350−450 km/s) represents 13,012 data points; and the "fast" PDF (>450 km/s) represents 9,116 data points. In each of the plots above, we limit our consideration to ratios of less than 4.0.

450 km/s), and fast ($>$ 450 km/s) solar wind. For $v < 350$ km/s, we find the mean value of $N_{\mathrm{DSCOVR}}/N_{Wind}$ to be 0.78 ± 0.27. At moderate speeds, it rises to 1.07 ± 0.73, and for $v > 450$ km/s, it becomes 1.8 ± 1.06. If we restrict our focus to ratios of less than 4.0, we find means of 0.78 ± 0.21 for $v < 350$ km/s, 1.03 ± 0.35 for v between 350 and 450 km/s, and 1.69 ± 0.59 for $v > 450$ km/s. This narrower scope, selected to exclude extreme outliers, comprises 99.9% of the "slow" category, 99.5% of the "moderate" category, 97.5% of the "fast" category, and 99.0% of DSCOVR-*Wind* density ratios as a whole. Our results suggest that DSCOVR tends to underestimate the proton density when the solar wind speed is low and overestimate it when the solar wind speed is high, while DSCOVR and *Wind* provide comparable density measurements when the solar wind speed is moderate. Normalized Probability density functions for each speed bin are displayed in Figure 9 (bottom).

A parallel (though weaker) trend is observed among DSCOVR-*Wind* temperature ratios (plot not shown here). For ratios less than 4.0, we find for low solar wind speeds a mean $T_{\mathrm{DSCOVR}}/T_{Wind}$ value of 0.86 ± 0.44; for moderate speeds 1.51 ± 0.87; and for high speeds 2.02 ± 0.86. In this case, this accounts for 92.9% of the "slow" bin, 90.9% of the "moderate" bin, 87.6% of the "fast" bin, and 90.5% of $T_{\mathrm{DSCOVR}}/T_{Wind}$ values overall. Results obtained using the full set can be found in Table 4.

When we sort the DSCOVR-*Wind* v_x ratios by *Wind* speed, we find means close to unity with minimal spread for each bin. However, no dependencies were found for v_y and v_z ratios. Likewise, we found no clear speed dependence among B_z ratios. We note that the spreads in $B_{z,\,\mathrm{DSCOVR}}/B_{z,\,Wind}$ are fairly large, and so the averages we report should not be taken as conclusive evidence of a tendency for DSCOVR to underestimate B_z measurements. See Table 4 for details.

We repeat this analysis for proton density, sorting DSCOVR-*Wind* ratios into low- and high-density bins ($\leq$ 5/cc and $>$ 5/cc, respectively) based on the *Wind* measurements. At low densities, $N_{\mathrm{DSCOVR}}/N_{Wind} = 1.62 \pm 1.19$ on average, compared with 0.92 ± 0.27 at high densities (see Figure 9). If we implement the 4.0 ratio threshold, the mean $N_{\mathrm{DSCOVR}}/N_{Wind}$ value falls to 1.49 ± 0.66 for low density; the high-density value is unchanged. Density ratios of less than 4.0 comprise 97.6% of the "low-density" bin and 100% of the "high-density" bin. Shifting our focus to temperature and limiting $T_{\mathrm{DSCOVR}}/T_{Wind}$ to less than 4.0, we find means of 1.97 ± 0.98 for $N_{Wind} \leq 5$/cc (representing 83.2% of the "low-density" bin), compared to 1.17 ± 0.65 for $N_{Wind} > 5$/cc (representing 95.4% of the "high-density" bin). This suggests that DSCOVR tends to overestimate both density and temperature when the ambient proton density is low, while its measurements of these parameters are more likely to agree with *Wind* at higher densities.

We observe, as we would again expect, that DSCOVR and *Wind* v_x values are comparable across density bins. Moreover, there is no discernible density dependence in either v_y, v_z, or B_z. As before, the large spreads in $B_{z,\,\mathrm{DSCOVR}}/B_{z,\,Wind}$ values limit the utility of this particular finding. Results are summarized in Table 5. Below we discuss these results and provide concluding statements.

5 Discussions and Conclusions

In this study we validated DSCOVR MAG and FC data against equivalent *Wind* and ACE science data. DSCOVR magnetic field observations show good statistical agreement with *Wind* and ACE measurements over the period studied. IMF-B_z showed the lowest correlation for all three satellite comparisons (see bottom panel of Figure 4). Signs of significant degradation over time using monthly values were inconclusive between DSCOVR-*Wind* B_z, although this monthwise analysis was not repeated for *Wind*-ACE.

The results in Table 3 indicating that agreement between DSCOVR and *Wind* B_z measurements improves when the satellites are closer is interesting, as it suggests that

Table 4. Means and standard deviations of DSCOVR-*Wind* ratios for proton density, temperature, solar wind v_x (GSE), and B_z (GSE), classified into three bins based on solar wind speed (as measured by *Wind*). Ratios are computed from hourly averages spanning the full range of this analysis (2016−2020). Italicized values are the results when we limit our focus to ratios of magnitude less than 4.0.

	$N_{\text{DSCOVR}}/N_{Wind}$	$T_{\text{DSCOVR}}/T_{Wind}$	$v_{x,\text{DSCOVR}}/v_{x,Wind}$	$B_{z,\text{DSCOVR}}/B_{z,Wind}$
<350 km/s	0.78 ± 0.27	1.69 ± 4.54	1.02 ± 0.16	0.91 ± 19.61
	0.78 ± 0.21	*0.86 ± 0.44*	*1.02 ± 0.16*	*0.79 ± 0.99*
$350-450$ km/s	1.07 ± 0.73	1.99 ± 2.1	1.02 ± 0.04	0.63 ± 40.15
	1.03 ± 0.35	*1.51 ± 0.87*	*1.02 ± 0.04*	*0.79 ± 1.02*
>450 km/s	1.8 ± 1.06	2.48 ± 1.66	1.01 ± 0.03	0.7 ± 80.7
	1.69 ± 0.59	*2.02 ± 0.86*	*1.01 ± 0.03*	*0.74 ± 1.08*

Table 5. Means and standard deviations of DSCOVR-*Wind* ratios for proton density, temperature, solar wind v_x (GSE), and B_z (GSE), classified into two bins based on proton density (as measured by *Wind*). Ratios are computed from hourly averages spanning the full range of this analysis (2016−2020). Italicized values are the results when we limit our focus to ratios of magnitude less than 4.0.

	$N_{\text{DSCOVR}}/N_{Wind}$	$T_{\text{DSCOVR}}/T_{Wind}$	$v_{x,\text{DSCOVR}}/v_{x,Wind}$	$B_{z,\text{DSCOVR}}/B_{z,Wind}$
≤ 5/cc	1.62 ± 1.19	2.79 ± 3.36	1.02 ± 0.11	1.03 ± 60.29
	1.49 ± 0.66	*1.97 ± 0.98*	*1.02 ± 0.1*	*0.73 ± 1.09*
>5/cc	0.92 ± 0.27	1.55 ± 2.5	1.01 ± 0.08	0.53 ± 45.68
	0.92 ± 0.27	*1.17 ± 0.65*	*1.01 ± 0.08*	*0.8 ± 0.98*

IMF-B_z observations are somewhat sensitive to spacecraft orbit parameters at L1. This was also found by King and Papitashvili (2005), who presented a statistical comparison of ACE and Wind solar wind data from NASA-CDAWeb. King and Papitashvili included the effect of spacecraft separation on their cross-satellite comparisons by implementing an impact parameter (IP), defined therein *as the distance by which a downstream spacecraft misses seeing a plasma element previously seen by an upstream spacecraft.* IP is a function of spacecraft position vector (x_i, y_i, z_i, where i is the spacecraft 1 or 2) and can be calculated from $\sqrt{[(y_1 - y_2) + (x_1 - x_2)/13]^2 + (z_1 - z_2)^2}$, assuming a radial solar wind speed of 390 km/s. They also utilized weighted regressions, in which the slope and intercept of the linear trend line are determined by minimizing a chi-square function. We incorporated King and Papitashvili's IP threshold and weighting protocol in our analysis (results are not presented here) but no appreciable improvement in either trend line equations or Pearson's r values was found.

Previous studies show that IMF parameters are better correlated over spatial scales during solar active periods compared to quiet solar times (Collier et al., 1998; King & Papitashvili, 2005). Since the data period for analysis was taking from the declining phase of Solar cycle 24 as the cycle moved towards minimum, this may explain the negative correction between DSCOVR and *Wind* B_z measurements with satellite separation. Further analysis based on spatial scales is beyond the scope of this study. However, given the importance of solar wind parameters (particularly the IMF) in space weather prediction and forecasting, we recommend more studies be undertaken to better inform of the dependency of L1 observations on spacecraft separation and spatial scales.

The results for the DSCOVR FC solar wind particle comparisons to *Wind* and ACE are more mixed. The v_y and v_z components of the solar wind can influence space weather, for example, the orientation of the geomagnetic tail and consequently the regions of space, and tail processes, that surround satellites in that region. However, the solar wind bulk speed is dominated by the v_x-component, as seen in Figure 5. In other words, the solar wind is mainly radial. Hence, the resulting lower correlation for v_y and v_z is less consequential on space weather forecasting capabilities.

For individual days, there are times where DSCOVR v_x measurements deviated significantly from *Wind* and ACE (see Figure 8). This tends to happen when *Wind* and ACE v_x measurements are low, as shown in the top panels of Figure 5. The root cause is electrical grounding issues with the FC, which results in difficulty resolving solar wind peak amplitudes and inaccuracies in background subtractions during low solar wind conditions.

Our analysis of density ratios also indicates that statistically there is a dependency of solar wind speed (slow, medium or fast) on whether DSCOVR density estimates are below *Wind*, about equal to *Wind*, or higher than *Wind* density measurements. The medium solar wind speed (350-450 km/s) seems to be a sweet spot where DSCOVR and *Wind* density estimates are about equal, while DSCOVR density observations tend to overestimate compared to *Wind* when solar wind densities are low (below ∼5 cc).

Overall, the DSCOVR density calculations showed good agreement with *Wind* and ACE and also better correlations than for temperature. The temperature being a second-order moment statistically amplifies errors associated with lower-order estimates such as density. Therefore it is not surprising that correlations were lowest for temperature. Faraday Cups are tuned to velocity distributions, and with v_x dominating the solar wind speed, we also expected that v_x would show the best correlation. However, the moments estimates assumes the proton velocity distribution function (VDF) is isotropic because the algorithm uses a 1-D VDF. There are often anisotropic conditions which make this assumption less valid.

The DSCOVR data used in this study is the NCEI archive of real-time NOAA DSCOVR space weather operational data. This dataset has not been reprocessed, like ACE and *Wind* data, to improve data quality and science quality. For operations, a simple robust moments method (Stevens et al., 2014) was employed for DSCOVR solar wind parameter estimations. However, reprocessed 1-minute resolution FC dataset using a nonlinear fitting method and covering time periods in 2016-2019 is available on the NASA-CDAWeb. The DSCOVR space weather data, particularly with ACE aging well beyond its operational mission lifetime, provides an important contribution to both NOAA's space weather operations and space weather research in the science community.

Acknowledgments

This work was supported by the NOAA Cooperative Agreement with CIRES-University of Colorado, NA17OAR4320101. The views, opinions, and findings contained in this report are those of the authors and should not be construed as an official National Oceanic and Atmospheric Administration, National Aeronautics and Space Administration, or other U.S. Government position, policy, or decision.

Open Research

Data Availability Statement

Space weather data from NOAA's DSCOVR spacecraft, archived with identifiers at the NOAA-NCEI (NOAA, 2016), were used in the creation of this manuscript. Also used in this creation of this manuscript were magnetic field and particle data from the *Wind* spacecraft, which are archived and have identifiers as described by Koval et al. (2021) and Lazarus et al. (2021), respectively. Access to the ACE magnetic field and particle data used in the creation of this manuscript are described at `https://hpde.io/NASA/NumericalData/ACE/MAG/L2/PT1H` and `https://hpde.io/NASA/NumericalData/ACE/SWEPAM/L2/PT1H`, respectively. Data analysis were accomplished using the Python programming language [`https://www.python.org`] and figures were also created using Python. All Python releases are Open Source (see `https://opensource.org/` for the Open Source Definition).

References

Belcher, J. W. (1973). A variation of the davis-smith method for in-flight determination of spacecraft magnetic fields. *Journal of Geophysical Research (1896-1977)*, *78*(28), 6480-6490. Retrieved from `https://agupubs.onlinelibrary.wiley.com/doi/abs/10.1029/JA078i028p06480` doi: https://doi.org/10.1029/JA078i028p06480

Belcher, J. W., Davis Jr., L., & Smith, E. J. (1969). Large-amplitude alfvén waves in the interplanetary medium: Mariner 5. *Journal of Geophysical Research (1896-1977)*, *74*(9), 2302-2308. Retrieved from `https://agupubs.onlinelibrary.wiley.com/doi/abs/10.1029/JA074i009p02302` doi: https://doi.org/10.1029/JA074i009p02302

Biesecker, D., & Johnson, J. (2018). Dscovr – status update and comparing data from l1. In *The space weather workshop 2018*.

Boggs, P. T., Spiegelman, C. H., Donaldson, J. R., & Schnabel, R. B. (1988). A computational examination of orthogonal distance regression. *Journal of Econometrics*, *38*(1), 169-201. Retrieved from `https://www.sciencedirect.com/science/article/pii/0304407688900322` doi: https://doi.org/10.1016/0304-4076(88)90032-2

Collier, M. R., Slavin, J. A., Lepping, R. P., Szabo, A., & Ogilvie, K. (1998). Timing accuracy for the simple planar propagation of magnetic field structures in the solar wind. *Geophysical Research Letters*, *25*(14), 2509-2512. Retrieved from https://agupubs.onlinelibrary.wiley.com/doi/abs/10.1029/98GL00735 doi: https://doi.org/10.1029/98GL00735

Connerney, J. E. P. (2013). *(dscovr) project magnetometer calibration plan dscovr-mag-cal-0001 revision (3)* (Tech. Rep.). NASA Goddard Space Flight Center.

Davis, L. J., & Smith, E. J. (1968). The in-flight determination of spacecraft magnetic field zeros. *EOS Trans. AGU*, *49*(257).

Kasper, J., Case, A., & Szabo, A. (2013). *Design and early observations from the dscovr solar wind faraday cup* (Tech. Rep.). NASA Goddard Space Flight Center.

King, J. H., & Papitashvili, N. E. (2005). Solar wind spatial scales in and comparisons of hourly wind and ace plasma and magnetic field data. *J. Geophys. Res.*, *110*(A02104).

Koval, A., Lepping, R. P., & Szabo, A. (2021). *Wind magnetic field investigation (mfi) composite data.* [dataset]. NASA Space Physics Data Facility. Retrieved from https://doi.org/10.48322/av38-wn55 doi: 10.48322/av38-wn55

Lazarus, A. J., Candey, R. M., Kasper, J. C., Ogilvie, K. W., & Fitzenreiter, R. J. (2021). *Wind solar wind experiment (swe) thermal plamsa moments, key parameter (k0), 99 s data* [dataset]. NASA Space Physics Data Facility and the Massachusetts Institute of Technology, Center for Space Research. Retrieved from https://doi.org/10.48322/3zky-gy15 doi: 10.48322/3zky-gy15

NOAA. (2016). *Noaa space weather prediction center: Deep space climate observatory (dscovr)* [dataset]. NOAA National Centers for Environmental Information. Retrieved from http://doi.org/10.7289/V51Z42F7 doi: 10.7289/V51Z42F73

Ogilvie, K. W., Chornay, D. J., Fritzenreiter, R. J., Hunsaker, F., Keller, J., Lobell, J., ... Gergin, E. (1995). Swe, a comprehensive plasma instrument for the wind spacecraft. *Space Science Reviews*, *71*(1), 55–77. Retrieved from https://doi.org/10.1007/BF00751326 doi: 10.1007/BF00751326

Stevens, M. L., Kasper, J. C., Case, A., & Koval, A. (2014). *Dscovr faraday cup level 1b theoretical basis document* (Tech. Rep.). NASA Goddard Space Flight Center.

Szabo, A. (2014). Deep space climate observatory (dscovr). In *The 6th nasa space weather and robotic mission operations workshop.*

Szabo, A. (2015). Dscovr instrumentation capabilities and calibration test plan. In *The space weather workshop 2015.*

Szabo, A., & Koval, A. (2016). Dscovr magnetometer observations. In *The space weather workshop 2016.*